

ARTICLES

Back-action-evading transducing scheme for cryogenic gravitational wave antennas

C. Cinquegrana

Dipartimento di Fisica, Università di Roma "La Sapienza," Rome, Italy

E. Majorana

*Istituto Nazionale di Fisica Nucleare, Sezione di Roma, Rome, Italy
and Dipartimento di Fisica, Università di Catania, Catania, Italy*

P. Rapagnani and F. Ricci

*Dipartimento di Fisica, Università di Roma, "La Sapienza," Rome, Italy
and Istituto Nazionale di Fisica Nucleare, Sezione di Roma, Rome, Italy*

(Received 2 February 1993)

We present the design, development, and test of a resonant capacitive transducer for gravitational wave antennas suitable for back-action-evading measurements. We describe a detailed theoretical model of such a transducer, analyze the general requirements that it must satisfy, and report the results of some tests at low temperatures. We obtain on our prototype a good value of the mechanical merit factor (2.8×10^6), a satisfactory geometrical balance, and a good stability of the electrical and geometrical parameters. The bridge readout circuit was balanced down to 0.8 ppm and an electrical quality factor $Q_e \simeq 6 \times 10^3$ was measured for the electrical resonance at 123 kHz. The noise behavior of the system is in satisfactory agreement with the values predicted by our theoretical model.

PACS number(s): 04.80.+z, 06.70.Mx, 43.88.+q

I. INTRODUCTION

The explosion of supernovas (SN's) is thought to be the most powerful and best known source of gravitational waves (GW) at frequencies of about 1 kHz. However, the interaction of these GW signals with matter is extremely weak: a SN explosion at a distance of about 10^4 light years would yield a perturbation of the dimensionless metric tensor h of the order of 10^{-18} . This means that a body of 1 m length would change its linear dimension of 10^{-18} m. At present, this sensitivity has been reached by cryogenic gravitational wave antennas [1,2] currently developed by several groups around the world, and a long period of observations at this level has started [3]. However, the most reliable estimates of SN frequencies give a value of about 1 SN every 10–30 years [4] for our Galaxy. In order to have a rate of some SN explosions per year it is necessary to extend the range of observation to the nearest cluster of galaxies, the Virgo cluster, at about 10^7 light years, and so be able to observe signals which produce displacements of the order of 10^{-21} m at 1 kHz.

The energy sensitivity of a resonant detector is limited by its fundamental state quantum energy $h\nu$. At 1 kHz and for a mass of 1000 kg the minimum displacement which can be resolved is of the order of 10^{-20} . However, at this level of amplitude the gravitational wave exciting the antenna can be viewed as completely classical. Several authors have pointed out that quantum mechanics should impose no limit on measuring a truly classical

force (for an extensive review of the issues of the principle the reader is referred to the article by Caves *et al.* [5]). This has suggested to us that we devise several techniques for monitoring the motion of a resonant antenna beating its quantum limit. An extended theoretical treatment of this topic can be found in Refs. [6–8]. From these studies we soon recognized the possibility of implementing the quantum nondemolition (QND) scheme also in a purely classical framework, allowing us to overcome the standard energy resolution limit of a linear transduction configuration. In the fundamental paper of Giffard [9] it is shown that this limit is equal to $2T_n$, T_n being the noise temperature of the electronic amplifier coupled to the motion transducer. The QND technique achieves this result by avoiding the back action of the amplifier on the transduction circuit and thus has been called back action evasion (BAE) [10]. Several groups are currently developing BAE transducers for gravitational wave antennas [11–16]. In this work we present the design, development, and test of a new BAE transducing system for resonant gravitational wave antennas which uses a push-pull resonant capacitive transducer coupled to a high electrical Q circuit.

Section II deals with a quantitative model developed to study the influence of the noise sources on the system and predict its performance.

In Sec. III we discuss the general requirements that the parameters of the system must satisfy, we describe the design, construction, and assembling technique of the transducer and present some results of tests performed on

the transducer at low temperature.

Section IV deals with the development of the passive elements of the bridge circuit and with the static balancing of the readout bridge.

Section V presents the results of noise and sensitivity measurements performed at low temperature on the complete system and discuss the possible sensitivity which can be reached by coupling such a system to an antenna.

II. THEORETICAL MODEL OF A BAE TRANSDUCING SCHEME

A. Basic scheme of a BAE transducer

The most general scheme of a BAE transducer is shown in Fig. 1. The complete Hamiltonian of this system is

$$H_s = \frac{p^2}{2m} + \frac{1}{2} m \omega_m^2 x^2 + H_i + \frac{\phi^2}{2L} + \frac{1}{2} L \omega_e^2 q^2 - xF(t) - qR(t), \quad (2.1)$$

where $F(t)$ and $R(t)$ are the mechanical and electrical forcing terms, respectively, and H_i is an interaction Hamiltonian coupling a mechanical oscillator at frequency ω_m to an electrical oscillator at frequency $\omega_e \gg \omega_m$:

$$H_i = E(t)q(t)x, \quad (2.2)$$

where q is the electrical charge on the capacitance and $E(t)$ is the biasing electrical field of the motion transducer, having the shape

$$E(t)_{\text{BAE}} = E_0 \cos \omega_e t \cos \omega_m t. \quad (2.3)$$

This particular time dependence of the coupling electrical field permits us to obtain the back-action-evasion effect. In fact, if we write the Hamilton equations of the system in terms of the complex amplitudes of the mechanical and electrical oscillators,

$$\begin{aligned} X_2 + jX_1 &= (1/\omega_m)(\dot{x} + j\omega_m x) e^{-j\omega_m t}, \\ Q_2 + jQ_1 &= (1/\omega_e)(\dot{q} + j\omega_e q) e^{-j\omega_e t}, \end{aligned} \quad (2.4)$$

we obtain

$$\begin{aligned} \dot{X}_1 &= \frac{E(t)}{m\omega_m} \sin \omega_m t \cos \omega_e t Q_1 + \frac{E(t)}{m\omega_m} \sin \omega_m t \sin \omega_e t Q_2 \\ &\quad - \frac{F(t)}{m\omega_m} \sin \omega_m t, \\ \dot{X}_2 &= -\frac{E(t)}{m\omega_m} \cos \omega_m t \cos \omega_e t Q_1 - \frac{E(t)}{m\omega_m} \cos \omega_m t \sin \omega_e t Q_2 \\ &\quad + \frac{F(t)}{m\omega_m} \cos \omega_m t, \end{aligned} \quad (2.5)$$

$$\begin{aligned} \dot{Q}_1 &= \frac{E(t)}{L\omega_e} \cos \omega_m t \sin \omega_e t X_1 + \frac{E(t)}{L\omega_e} \sin \omega_m t \sin \omega_e t X_2 \\ &\quad - \frac{R(t)}{L\omega_e} \sin \omega_e t, \end{aligned}$$

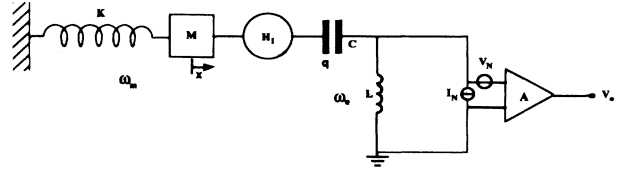


FIG. 1. General QND detection scheme.

$$\begin{aligned} \dot{Q}_2 &= -\frac{E(t)}{L\omega_e} \cos \omega_m t \cos \omega_e t X_1 - \frac{E(t)}{L\omega_e} \sin \omega_m t \cos \omega_e t X_2 \\ &\quad + \frac{R(t)}{L\omega_e} \cos \omega_e t. \end{aligned}$$

Taking into account the dynamic coupling (2.3), these equations show that a perturbation on Q_1 influences mostly X_2 , but leaves X_1 almost unaffected over periods $\Delta t \gg 2\pi/\omega_m, 2\pi/\omega_e$. In this situation the interaction Hamiltonian (2.2) assumes the form

$$H_i \approx E_0 X_1 Q_1. \quad (2.6)$$

However, in order to give a complete analytical treatment of this problem we must specify our operating setup, which is slightly more complicated than in Fig. 1. In fact, the vibration of the mechanical oscillator is usually detected by means of the two capacitors of a differential capacitive transducer inserted in a bridge configuration (see Fig. 2). The electrical oscillator is given by the resonance network of the capacitive bridge and the central arm coil. In this configuration, any noise coming from the biasing field sources (usually called em pumps) is reduced by a factor equal to the static impedance balancing of the bridge, η_z . The minimization of this parameter is essential to having a good sensitivity of the transducer, and is one of the main constraints to be taken into account in designing and developing the transduction circuit. On the other hand, the impedance of each arm of the bridge of Fig. 2 also has a resistive component that contributes to the overall balance. Hence, it is important to derive the conditions that the resistive terms in the impedances of the arms of the bridge must satisfy in order to neglect their effect on the balance.

In the following, we consider the circuit in Fig. 2, where now each element is represented by its capacitive and resistive terms:

$$Z_n = R_n + 1/j\omega C_n \quad \text{for } n = 1, 2, 3, 4. \quad (2.7)$$

The output voltage on the central arm due to a voltage V_p at the input is

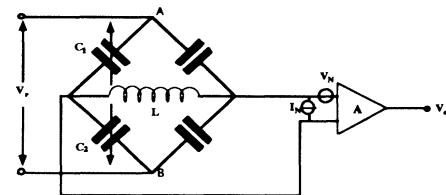


FIG. 2. BAE transduction scheme.

$$V_{\text{out}} = \frac{Z_2 Z_3 - Z_1 Z_4}{(Z_1 + Z_2)(Z_3 + Z_4)} V_p = \eta_z V_p . \quad (2.8)$$

For $\eta_z = 0$ we derive two conditions from the real and imaginary part of the impedance:

$$R_1 R_4 - R_2 R_3 + \frac{1}{\omega^2} \left[\frac{1}{C_2 C_3} - \frac{1}{C_1 C_4} \right] = 0 , \quad (2.9)$$

$$\frac{R_1}{C_4} + \frac{R_4}{C_1} - \frac{R_2}{C_3} - \frac{R_3}{C_2} = 0$$

that are satisfied for

$$\begin{aligned} R_1 R_4 &= R_2 R_3 , \\ C_1 C_4 &= C_2 C_3 , \\ R_1 C_1 &= R_3 C_3 . \end{aligned} \quad (2.10)$$

If we suppose to have both a capacitive and resistive unbalance, so that $C_1 = C_3 = C_4 = C$, $C_2 = C + \Delta C$, $R_1 = R_3 = R_4 = R$, $R_2 = R + \Delta R$, with $\omega_e R C \ll 1$, $\Delta R / R < 1$, $\Delta C / C \ll 1$, the factor η_z can be written as

$$\eta_z = \frac{1}{4} \omega C \left[\Delta R^2 + \left[\frac{\Delta C}{C} \right]^2 \frac{1}{\omega^2 C^2} \right]^{1/2} . \quad (2.11)$$

Equation (2.11) shows that it is possible to neglect the effect of the resistances in the bridge if

$$\Delta R \ll \frac{\Delta C}{C} \frac{1}{\omega C} . \quad (2.12)$$

Let us suppose that the residual value of η_z is due only to the resistive terms:

$$\Delta R = 4(\eta_z / \omega C) . \quad (2.13)$$

If we have $C \approx 1$ nF, $\omega_e \approx 2\pi 100$ kHz, and want $\eta_z \approx 10^{-7}$, we find

$$\Delta R \approx 10^{-3} \Omega . \quad (2.14)$$

This requirement can be met using superconducting wires for the connections of the elements and low loss dielectric materials for the capacitances. Thus, in the following we shall consider only the capacitive terms of our bridge circuit.

B. Equations of motion of the system

Let us now consider the transduction scheme shown in Fig. 2. We indicate with V_p the biasing voltage applied on the transducer through points *A* and *B* of the bridge.

We suppose that the capacitive bridge is out of balance because of a difference x_0 in the gap of the two capacitances C_1 and C_2 of the transducer. In this way we shall have a nonzero voltage V on the inductance L .

On the two capacitances C_1 and C_2 we have $\Delta V_{C_1} = V_p / 2 + V$, $\Delta V_{C_2} = V_p / 2 - V$. If

$$C_1 \approx C_2 \approx C = \epsilon_0 S / D ,$$

we have $E(t) = V_p(t) / D$, where D is the mean value of the gaps between the plates of the transducer. If the cen-

tral plate of the differential transducer vibrates, the charge variation $q(t)$ on C_1 and C_2 can be expressed as

$$q(t) = Q_1 - Q_2 = 2CV(t) . \quad (2.15)$$

Now we specify the forces acting on the system: on the mechanical oscillator acts the force due to the signal F_s , and the Langevin force F_n which causes the Brownian motion. The term $L\dot{I}_n$ takes into the account the effect of the current noise of the amplifier that originates the back action on the transduction circuit. Moreover, we introduce the dissipating terms of the two oscillators:

$$F_{dm} = -(m / \tau_m) \dot{x} , \quad F_{de} = -(L / \tau_e) \dot{q} , \quad (2.16)$$

where τ_m and τ_e are their characteristic energy relaxation times. So we have

$$F(t) = F_s + F_n + F_{dm} , \quad (2.17)$$

$$R(t) = L\dot{I}_n + F_{de} . \quad (2.18)$$

And the complete equations of motion of the complete system are

$$\ddot{x} + \frac{1}{\tau_m} \dot{x} + \omega_m^2 x + \frac{2C}{mD} V_p V = \frac{F_s + F_n}{m} - \omega_m^2 x_0 , \quad (2.19)$$

$$\ddot{V} + \frac{1}{\tau_e} \dot{V} + \omega_e^2 V + \frac{\omega_e^2}{2D} V_p x = \frac{1}{2C} \frac{dI_n}{dt} .$$

For a BAE transducer, the bias voltage $V_p(t)$ is

$$\begin{aligned} V_p &= (V_0 / 2) \{ \cos[(\omega_e + \omega_m)t + \theta_1] \\ &\quad + \cos[(\omega_e - \omega_m)t + \theta_2] \} , \end{aligned} \quad (2.20)$$

where θ_1 and θ_2 are the phase of the two em pumps with respect to a certain reference.

C. Response of the transducer to an impulsive force

In this section we shall compute the response of the system to an impulsive excitation. The result will be used later in the analysis of the sensitivity of this device. We again write Eqs. (2.19), where all the noise forcing terms are now set to zero:

$$\ddot{x} + \frac{1}{\tau_m} \dot{x} + \omega_m^2 x + \frac{2C}{mD} V_p V_s = \frac{F_s}{m} , \quad (2.21)$$

$$\ddot{V}_s + \frac{1}{\tau_e} \dot{V}_s + \omega_e^2 V_s + \frac{\omega_e^2}{2D} V_p x = -\eta_z \omega_e^2 V_p .$$

We have shifted the origin of the x axis so that it now coincides with x_0 and we have introduced the expression $\eta_z = x_0 / 2D$.

This system can be more easily solved using the new variables X_1 , X_2 , V_1 , and V_2 which are related to x , \dot{x} and V , \dot{V} by

$$\begin{aligned} X_2 + jX_1 &= \frac{1}{\omega_m} (\dot{x} + j\omega_m x) e^{-j\omega_m t} , \\ V_2 + jV_1 &= \frac{1}{\omega_e} (\dot{V} + j\omega_e V) e^{-j\omega_e t} . \end{aligned} \quad (2.22)$$

Substituting these expressions in system (2.21) and assuming $\theta_1 = \theta_2 = 0$ we obtain a set of four linear equations for the variables X_1, X_2, V_1 , and V_2 that assumes the following form by averaging over periods $\Delta t \gg 2\pi/\omega_m, 2\pi/\omega_e$:

$$\begin{aligned} \left[\frac{d}{dt} + \frac{1}{2\tau_m} \right] X_1 &= -\frac{F_s}{m\omega_m} \sin\omega_m t, \\ \left[\frac{d}{dt} + \frac{1}{2\tau_m} \right] \left[\frac{d}{dt} + \frac{1}{2\tau_e} \right] X_2 &= \left[\frac{d}{dt} + \frac{1}{2\tau_e} \right] \frac{F_s}{m\omega_m} \cos\omega_m t, \\ \left[\frac{d}{dt} + \frac{1}{2\tau_e} \right] V_1 &= 0, \\ \left[\frac{d}{dt} + \frac{1}{2\tau_e} \right] \left[\frac{d}{dt} + \frac{1}{2\tau_m} \right] V_2 &= - \left[\frac{d}{dt} + \frac{1}{2\tau_m} \right] \frac{\eta_z \omega_e V_0}{2} \cos\omega_m t \\ &\quad - \frac{\omega_e V_0 F_s}{8m\omega_m D} \sin\omega_m t. \end{aligned} \quad (2.23)$$

We solve this system with the hypothesis that the only driving force acting on the harmonic oscillator is an impulsive force arriving at the time $t = t_0$:

$$F_s \approx P_0 \delta(t - t_0). \quad (2.24)$$

For $t \geq t_0$ we obtain the solutions

$$X_1(t) = A_1 e^{-t/2\tau_m} - \frac{P_0 \sin\omega_m t_0 e^{t_0/2\tau_m}}{m\omega_m} e^{-t/2\tau_m}, \quad (2.25)$$

$$\begin{aligned} X_2(t) &= A_2 e^{-t/2\tau_m} + A_3 e^{-t/2\tau_e} \\ &\quad + \frac{P_0 \cos\omega_m t_0 e^{t_0/2\tau_m}}{m\omega_m} e^{-t/2\tau_m}, \end{aligned} \quad (2.26)$$

which give, for $x(t)$,

$$\begin{aligned} x(t) &= \left[A_2 + \frac{P_0 \cos\omega_m t_0 e^{t_0/2\tau_m}}{m\omega_m} \right] e^{-t/2\tau_m} \sin\omega_m t \\ &\quad + A_3 e^{-t/2\tau_e} \sin\omega_m t \\ &\quad + \left[A_1 - \frac{P_0 \sin\omega_m t_0 e^{t_0/2\tau_m}}{m\omega_m} \right] e^{-t/2\tau_m} \cos\omega_m t, \end{aligned} \quad (2.27)$$

$$x(t) = \frac{P_0}{m\omega_m} e^{-(t-t_0)/2\tau_m} \sin\omega_m(t-t_0), \quad (2.33)$$

$$\begin{aligned} V_s(t) &= \frac{Q_e V_0 P_0 \sin\omega_m t_0 \sin\omega_e t}{4Dm\omega_m} (e^{-(t-t_0)/2\tau_e} - e^{-(t-t_0)/2\tau_m}) \\ &\quad - \eta_z \frac{V_0}{4} \frac{\omega_e}{\omega_m} \left[\cos(\omega_e - \omega_m)t - \cos(\omega_e + \omega_m)t \right] - \frac{1}{2} \frac{1}{\omega_m \tau_e} [\sin(\omega_e - \omega_m)t + \sin(\omega_e + \omega_m)t]. \end{aligned} \quad (2.34)$$

These equations show that the system is phase sensitive. The response to the burst excitation depends on the phase of the pump voltage at the time of arrival.

while for V_1 and V_2 we find

$$V_1(t) = B_1 e^{-t/2\tau_e}, \quad (2.28)$$

$$\begin{aligned} V_2(t) &= \left[B_2 + \frac{Q_e V_0 P_0 \sin\omega_m t_0 e^{t_0/2\tau_e}}{4Dm\omega_m} \right] e^{-t/2\tau_e} \\ &\quad + \left[B_3 - \frac{Q_e V_0 P_0 \sin\omega_m t_0 e^{t_0/2\tau_m}}{4Dm\omega_m} \right] e^{-t/2\tau_m} \\ &\quad - \eta_z \frac{V_0}{2} \frac{\omega_e}{\omega_m} \sin\omega_m t - \eta_z \frac{V_0}{4} \frac{\omega_e}{\omega_m^2 \tau_e} \cos\omega_m t, \end{aligned} \quad (2.29)$$

where $Q_e = \omega_e \tau_e$ is the electric quality factor of the circuit. The three constants A_i are not completely independent to the B_i constants, as it is implied by the system (2.21). In fact, it can be shown, with a simple but tedious derivation that

$$A_3 = \frac{CV_0 \tau_e}{m\omega_m D} B_1, \quad B_3 = \frac{Q_e V_0}{4D} A_1. \quad (2.30)$$

The remaining constants are defined by imposing the initial conditions

$$x(t=0) = 0, \quad \dot{x}(t=0) = 0, \quad (2.31)$$

$$V(t=0) = 0, \quad (2.32)$$

$$\begin{aligned} \dot{V}(t=0) &= -\eta_z \frac{V_0}{8} \frac{\omega_e}{\omega_m^2 \tau_e} (\omega_e - \omega_m) \\ &\quad - \eta_z \frac{V_0}{8} \frac{\omega_e}{\omega_m^2 \tau_e} (\omega_e + \omega_m). \end{aligned}$$

The physical meaning of the boundary conditions (2.31) is evident. The boundary conditions (2.32) are derived from the residual current flowing through the central arm also in absence of a signal because of the imperfect balance of the bridge.

We finally obtain the response of the system to an impulsive force

D. Noise spectrum at the output of the transducer

In this section we solve the complete system of equations of our parametric transducer and we find the shape of the noise spectrum at the output of the transducer. In order to evaluate the noise response of the BAE transducer, we have to take into account the noise contribution in the coupling terms that appear in the two equations (2.19):

$$(2C/mD)V_p V, \quad \left(\frac{\omega_e^2}{2D}\right)V_p x, \quad (2.35)$$

where now V and x are the sum of the corresponding noise and signal terms: $V=V_n+V_s$ and $x=x_n+x_s$. In order to evaluate the noise output, the contribution due to the amplitude and phase fluctuation of the em pumps must also be included:

$$V_p(T) = (V_0/2)\{(1+a_1)\cos[(\omega_e+\omega_m)t+\theta_1+\phi_1] \\ + (1+a_2)\cos[(\omega_e-\omega_m)t-\theta_2+\phi_2]\}, \quad (2.36)$$

where a_1, a_2, ϕ_1 , and ϕ_2 are the stochastic fluctuations of the em pumps in amplitude and phase. We assume that the stochastic variables have a constant power spectrum and are not cross related. Under this assumption, we approximate the two terms (2.35) as

$$\frac{2C}{mD}V_p V \rightarrow \frac{2C}{mD}(V_p V + V_{p_n} V_s), \quad (2.37)$$

where

$$V_{p_n} = (V_0/2)[a_1\cos(\omega_e+\omega_m)t - \phi_1\sin(\omega_e+\omega_m)t \\ + a_2\cos(\omega_e-\omega_m)t - \phi_2\sin(\omega_e-\omega_m)t] \quad (2.38)$$

is the noise voltage of the pumps, while V_s in the case of an impulsive signal is given in formula (2.34).

In a similar way

$$\frac{\omega_e^2}{2D}V_p x \rightarrow \frac{\omega_e^2}{2D}(V_p x_n + V_{p_n} x_s). \quad (2.39)$$

It follows that the equations describing the noise behavior of the transducer are

$$\ddot{x}_n + \frac{1}{\tau_m}\dot{x}_n + \omega_m^2 x_n + \frac{2C}{mD}V_p V_n = \frac{F_n}{m} - \frac{2C}{mD}V_{p_n} V_s, \quad (2.40) \\ \ddot{V}_n + \frac{1}{\tau_e}\dot{V}_n + \omega_e^2 V_n + \frac{\omega_e^2}{2D}V_p x_n = \frac{1}{2C}\frac{dI_n}{dt} - \eta_z \omega_e^2 V_{p_n} \\ - \frac{\omega_e^2}{2D}V_{p_n} x.$$

As for the general scheme of a BAE transducer we derive the corresponding linearized equations for the variables X_1, X_2, V_1 , and V_2 :

$$\left(\frac{d}{dt} + \frac{1}{2\tau_m}\right)X_1 = n_1, \\ \left(\frac{d}{dt} + \frac{1}{2\tau_m}\right)\left(\frac{d}{dt} + \frac{1}{2\tau_e}\right)X_2 \\ = \left(\frac{d}{dt} + \frac{1}{2\tau_e}\right)n_2 - \frac{V_0 C}{2m\omega_m D}n_3, \quad (2.41)$$

$$\left(\frac{d}{dt} + \frac{1}{2\tau_e}\right)V_1 = n_3, \\ \left(\frac{d}{dt} + \frac{1}{2\tau_e}\right)\left(\frac{d}{dt} + \frac{1}{2\tau_m}\right)V_2 \\ = \left(\frac{d}{dt} + \frac{1}{2\tau_m}\right)n_4 + \frac{\omega_e V_0}{8mD}n_1,$$

where

$$n_1 = \frac{F_n}{m\omega_m}\sin\omega_m t + \frac{2C}{m\omega_m D}V_s V_{p_n}\sin\omega_m t \\ + \frac{CV_0}{4m\omega_m D}[(a_2-a_1)V_2 + (\phi_2-\phi_1)V_1], \quad (2.42a)$$

$$\eta_2 = \frac{F_n}{m\omega_m}\cos\omega_m t - \frac{2C}{m\omega_m D}V_s V_{p_n}\cos\omega_m t \\ + \frac{CV_0}{4m\omega_m D}[(\phi_2+\phi_1)V_2 - (a_2+a_1)V_1], \quad (2.42b)$$

$$n_3 = -\left[\frac{\dot{I}_n}{2C\omega_e} - \eta_z \omega_e V_{p_n}\right]\sin\omega_e t + \frac{\omega_e x}{2D}V_{p_n}\sin\omega_e t \\ + \frac{\omega_e V_0}{16D}[(a_2-a_1)X_2 - (\phi_2+\phi_1)X_1], \quad (2.42c)$$

$$n_4 = -\left[\frac{\dot{I}_n}{2C\omega_e} - \eta_z \omega_e V_{p_n}\right]\cos\omega_e t - \frac{\omega_e x}{2D}V_{p_n}\cos\omega_e t \\ + \frac{\omega_e V_0}{16D}[(\phi_2-\phi_1)X_2 + (a_2+a_1)X_1]. \quad (2.42d)$$

We notice that all the equations are coupled due to the presence of the noise terms. Further, the quantities n_1, n_2, n_3 , and n_4 also include terms that depend on the product of the output variables X_1, X_2, V_1 , and V_2 times the noise fluctuation of the pumps. As we look for small signal solutions of the system (2.41), we shall treat these terms as a system perturbation. A consistency check can be done comparing this contribution with those due to the Brownian motion and the pump fluctuation. In order to obtain the noise spectrum of the transducer output we have to solve the system (2.41) in the frequency domain by introducing for each stochastic variable the corresponding bilateral noise power spectrum.

An extensive presentation of the algebra procedure is presented in Ref. [17]. Here we report the results, recalling that the derivation relies on two fundamental assumptions: (a) we assume that the readout circuit is able

to filter the $2\omega_e$ terms and the higher harmonics that arise when we introduce the power spectrum of the quantities $V_{p_n} \cos \omega_e t$ and $V_{p_n} \sin \omega_e t$; (b) all the sources of noise considered, such as the phase and amplitude noise of the

pumps, the current and voltage noise of the amplifier, and the thermal noise of the mechanical oscillator, are uncorrelated.

We obtain

$$Sn_1 \approx Sn_2 \approx \frac{k_b T}{m \omega_m^2 \tau_m} + \left[\frac{\eta_z \beta D \omega_e}{8} \right]^2 \left[S_a + \frac{S_\phi}{(2\omega_m \tau_e)^2} + \frac{\omega_m^2 \tau_e}{2} (S_a + S_\phi)^2 \right], \quad (2.43)$$

$$Sn_3 \approx Sn_4 \approx \frac{SI_n}{8C^2} + \frac{(\eta_z \omega_e V_0)^2}{16} (S_a + S_\phi), \quad (2.44)$$

where we have assumed that $S_{f_n} = 2k_b T_m / \tau_m$ is the bilateral noise spectrum of the Langevin force, S_a and S_ϕ are the amplitude and phase noise spectrum of the pumps, and β is the energy coupling factor of the transducer defined as

$$\beta = CV_0 / m \omega_m^2 D^2. \quad (2.45)$$

It follows that the spectra of the measured quantities V_1 and V_2 are

$$SV_1 = \frac{SI_n / 8C^2 + [(\eta_z \omega_e V_0)^2 / 16] (S_a + S_\phi)}{\omega^2 + 4\tau_e^2} + SV_n, \quad (2.46)$$

$SV_1 = (\text{amplifier white noise}) + (\text{amplifier} + \text{pumps wideband noise}),$

$$SV_2 = SV_1 + \frac{\left[\frac{V_0 \omega_e}{8D} \right]^2 \left[\frac{k_b T}{m \omega_m^2 \tau_m} + \left[\frac{\eta_z \beta D \omega_e}{8} \right]^2 \left[S_a + \frac{S_\phi}{2\omega_m \tau_e} + \frac{\omega_m^2 \tau_e}{2} (S_a + S_\phi)^2 \right] \right]}{\left[\omega^2 + \frac{1}{4\tau_m^2} \right] \left[\omega^2 + \frac{1}{4\tau_e^2} \right]}, \quad (2.47)$$

$SV_2 = SV_1 + (\text{Brownian motion} + \text{pumps narrow band noise}).$

In these equations we have also taken into account the contribution of the white voltage noise of the amplifier, which must be added to each spectrum.

We would like to stress the different influence of the noise on the two phase components at the output. On phase V_1 we have two different contributions: a white-noise term due to the amplifier, and a wide band noise term, present at the bandwidth of the electrical resonance of the readout circuit, due to the amplifier and the pumps.

On the V_2 component the same noise terms of phase V_1 are present with the addition of a narrow band term centered at ω_e . This last term has the typical bandwidth of the mechanical resonance and it is composed by the contributions of the signal due to the Brownian motion and the residual noise terms due to the pumps. If the balance of the bridge is such as to make negligible the noise of the pumps, the narrow band term is due only to the

Brownian motion of the mechanical oscillator, at its thermodynamical temperature: no back action noise from the amplifier is present. This is due to the back-action-evasion nature of our detection scheme.

In order to detect V_1 and V_2 a phase-sensitive technique is used. The signal is sent at the input of a lock-in amplifier, driven at the electrical frequency ω_e and referred to the same master oscillator of the two pumps. The transfer function of a lock-in amplifier of integration time τ_0 is

$$S_{11} = \frac{\tau_0^2}{1 + \omega^2 \tau_0^2} S_{vv}. \quad (2.48)$$

Thus, at the output of the lock-in we obtain two output signals that correspond to the two spectra of V_1 and V_2 integrated over the bandwidth of the lock-in. The variances of the two output processes will be

$$\sigma_1^2 = R_{11}(0) = \frac{2SV_n}{\tau_0} + \frac{2Q_e^2}{2\tau_e + \tau_0} \left[\frac{1}{8} \frac{SI_n}{(\omega_e C)^2} + \left[\frac{\eta_z V_0}{4} \right]^2 (S_a + S_\phi) \right], \quad (2.49)$$

$$\begin{aligned} \sigma_2^2 = R_{22}(0) = & \sigma_1^2 + \frac{(Q_e V_0)^2}{16} \frac{1}{\tau_m^2} \frac{\tau_e^2 \tau_0^2}{\tau_0^2 - 4\tau_e^2} \left[\tau_m \frac{\bar{x}_b^2}{D^2} + \left[\frac{\eta_z \beta \omega_e \tau_m}{8} \right]^2 \left[S_a + \frac{S_\phi}{(2\omega_m \tau_e)^2} + \frac{\omega_m^2 \tau_e}{2} (S_a + S_\phi)^2 \right] \right] \\ & \times \left[\tau_m \left[\frac{1}{\tau_e^2} - \frac{4}{\tau_0^2} \right] + \left[\frac{\tau_e}{\tau_0^2} - \frac{\tau_0}{2\tau_e^2} \right] \right]. \end{aligned} \quad (2.50)$$

E. Energy sensitivity of the transducer

We have shown in the previous sections that the response of the system to a mechanical excitation is contained in one (e.g., V_2) component of the complex electrical output signal. Moreover, the peculiarity of this phase sensitivity is that two more noise terms are present, both having the spectrum bandwidth of the mechanical resonance. These two terms, experimentally undistinguishable from the thermal noise, can be referred to the mechanical oscillator and regarded as additional noise forces. As it is usually done in the sensitivity analysis of a gravitational wave detector, an equivalent equipartition temperature of the system can be defined that, in this case, is related to only one phase of the transducer output. And, using the equation (2.50) we have

$$T_{\text{eq}} = T \left\{ 1 + \eta_z^2 \beta^2 \left[\frac{D\omega_e}{8} \right]^2 \frac{m\omega_m^2 \tau_m}{k_b T} \left[\left[S_a + \frac{S_\phi}{(2\omega_m \tau_e)^2} \right] + \frac{\omega_m^2 \tau_e}{2} (S_a + S_\phi)^2 \right] \right\}. \quad (2.51)$$

From this equation it follows that if the second term is made negligible with respect to 1, either lowering the pump noise or obtaining a low value for η_z , then there is no back action of the amplifier on the mechanical oscillator. T_{eq} can be regarded as a measure of the energy sensitivity of the detector. For the detection of burst signals the energy variation sensitivity is more significant. The usual way to evaluate this sensitivity in the research community involved in gravitational wave experiments is to introduce an effective temperature of the detector T_{eff} . In this case, T_{eff} will be obtained by optimizing the signal-to-noise ratio S/N on the sensitive phase of the detector.

Following the general theory of data analysis (see, for instance, Ref. [18]), the general expression for the signal-to-noise ratio verifies the inequality

$$\left[\frac{S}{N} \right]^2 = \frac{|V_{2_s}(t_0)|^2}{E(|V_{2_n}(t_0)|^2)} \leq \frac{1}{2\pi} \int_{-\infty}^{+\infty} \frac{|H(\omega)|^2}{SV_2(\omega)} d\omega, \quad (2.52)$$

where $H(\omega)$ represents the transfer function of the optimum filter that we are trying to derive.

In order to introduce the effective temperature we assume that S/N is equal to 1 and we maximize the response of the system for an impulsive signal. That releases an energy in the antenna given by

$$k_b T_{\text{eff}} = P_0^2 / 2m. \quad (2.53)$$

Thus, we obtain the compact expression for the effective

$$H_1 = Z_n \left[\frac{1}{4\tau_m^2} + \frac{1}{4\tau_e^2} \right] + \left[\frac{1}{8Z_n C^2} + \frac{\eta_z^2 V_0^2 \omega_e^2}{16k_b T_n} (S_a + S_\phi) \right], \quad (2.58)$$

$$H_2 = Z_n \frac{1}{16\tau_m^2 \tau_e^2} + \frac{1}{4\tau_m^2} \left[\frac{1}{8Z_n C^2} + \frac{\eta_z^2 V_0^2 \omega_e^2}{16k_b T_n} (S_a + S_\phi) \right] + \frac{V_0^2 \omega_e^2}{64k_b T_n D^2} \left[\frac{k_b T}{m\omega_m^2 \tau_m} + \left[\frac{\eta_z \beta D \omega_e}{8} \right]^2 \left[S_a + \frac{S_\phi}{(2\omega_m \tau_e)^2} + \frac{\omega_m^2 \tau_e}{2} (S_a + S_\phi)^2 \right] \right]. \quad (2.59)$$

temperature:

$$T_{\text{eff}} = T_n \frac{\omega_m}{\omega_e} \frac{1}{r}, \quad (2.54)$$

where

$$T_n = \frac{\sqrt{SV_n SI_n}}{k_b} \quad (2.55)$$

is the noise temperature of amplifier and

$$r = \left[\frac{\omega_e V_0^2 \sin^2 \omega_m t_0}{32m\omega_m D^2} \right] \frac{1}{2\pi} I \quad (2.56)$$

is the gain of the BAE configuration. This equation is obtained using, in Eq. (2.52), the impulsive response of the system given by Eq. (2.34), and the expression for the spectral density of the noise in Eq. (2.47). As discussed in Sec. II C, Eq. (2.56) shows that the sensitivity gain of the BAE coupling is maximum if the arrival time of the pulse coincides with the time of zero crossing of the pumping voltage V_p . The explicit expression of r is rather complex and in the following we report the definition of all the quantities that appear in it:

$$I = \left\{ \frac{2\pi^2}{H_1^2 - 4Z_n H_2} \left[\frac{Z_n}{2H_1} - \left[\frac{Z_n}{H_2} \right]^{1/2} \right] \right\}^{1/2}, \quad (2.57)$$

where $Z_n = \sqrt{SV_n/SI_n}$ is the noise impedance of the amplifier and

The transfer function of the optimum filter is obtained by fitting the condition

$$H(\omega) = k \frac{V_2^*(\omega)}{SV_2(\omega)} e^{-j\omega t_0} \quad (2.60)$$

and then the filtered data in the frequency domain are given by

$$V_2^f(\omega) = H(\omega)V_2(\omega)e^{j\omega t_0} = k \frac{|V_2(\omega)|^2}{SV_2(\omega)}. \quad (2.61)$$

Finally, from the above formula (2.61), the equivalent bandwidth of the detector can also be computed,

$$W = \frac{\int_{-\infty}^{+\infty} V_2^f(\omega) d\omega}{V_2^f(\omega = \omega_e)} = IH_2, \quad (2.62)$$

which corresponds to the inverse of the optimum integration time:

$$t_{\text{opt}} = 2\pi/W. \quad (2.63)$$

F. BAE transduction scheme with a resonant transducer

Up to this point, we have considered the BAE transducing scheme applied only to the parametric detection of the complex amplitude of one harmonic oscillator. However, it is well known that a considerable improvement in the sensitivity of a resonant gravitational wave antenna is obtained using a resonant transducer. In this device, the motion of a small resonator, vibrating at the same frequency of the bar, is detected. An antenna equipped with a resonant transducer can be well represented by a simple system [19] of a double harmonic oscillator in a series (Fig. 3). In order to use BAE detection on such a system, one must be certain that the new observed variable (i.e., the complex amplitude of the smaller oscillator) is indeed of the QND type. Moreover, it is crucial to find how to extend the previous analysis to the double oscillator system.

A pioneering treatment of this problem can be found in Ref. [11], and a more complete analysis is presented in Ref. [20], where the exact nature of the QND variables for a double oscillator system is demonstrated. In the following, we reexamine all of these considerations in view of their application to our transduction setup.

The Hamiltonian of a system of two harmonic oscillators as modeled in Fig. 3 is

$$H_{\text{DO}} = \frac{p_x^2}{2m_x} + \frac{1}{2}m_x\omega_x^2x^2 + \frac{p_y^2}{2m_y} + \frac{1}{2}m_x\omega_x^2(y-x)^2 \quad (2.64)$$

This system has two degrees of freedom, and thus it has

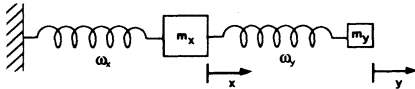


FIG. 3. Scheme of a double oscillator system.

two normal modes of vibration. Defining $\mu = m_y/m_x$, with ν_x and ν_y the frequencies of the uncoupled oscillators, it can be shown that the frequencies of the two normal modes of the system are

$$\nu_{\pm} = \left(\frac{1}{2} \{ \nu_y^2(1+\mu) + \nu_x^2 \} \pm \sqrt{[\nu_y^2(1+\mu) + \nu_x^2]^2 - 4\nu_x^2\nu_y^2} \right)^{1/2}. \quad (2.65)$$

A complete description of the system is also given in terms of its normal modes. In this case, the Hamiltonian can be written as the sum of the Hamiltonian of uncoupled harmonic oscillators, each one having the frequencies of the modes and proper equivalent masses and normal coordinates for the displacement.

For the double oscillator, the Hamiltonian is

$$H_{\text{DO}} = \frac{p_+^2}{2m_+} + \frac{1}{2}m_+\omega_+^2\xi_+^2 + \frac{p_-^2}{2m_-} + \frac{1}{2}m_-\omega_-^2\xi_-^2, \quad (2.66)$$

where the equivalent masses of the two modes are

$$m_{\pm} = \frac{m_x + \lambda_{\pm}^2 m_y}{(\lambda_{\pm} - 1)^2}, \quad (2.67)$$

where we have

$$\lambda_{\pm} = \frac{\nu_y^2}{\nu_y^2 - \nu_{\pm}^2} \quad (2.68)$$

and the two reduced normal coordinates ξ_- and ξ_+ are related to x and y by the relations

$$\xi_{\pm} = \frac{\pm(x\lambda_{\mp} - y)(\lambda_{\pm} - 1)}{\lambda_- - \lambda_+}. \quad (2.69)$$

The output of the antenna-transducer system is a function of the quantity $y - x$, that in terms of the normal coordinates assumes the simple form

$$y - x = \xi_+ + \xi_- . \quad (2.70)$$

As shown in Ref. [19], all the considerations done for the single oscillator apply to the system of two uncoupled oscillators. The physical variable which is monitored in a resonant BAE transducer is the differential displacement between the first and second mass ($y - x$), and the interaction Hamiltonian which couples the electrical readout oscillator to the double mechanical oscillator, is

$$H_i = E(t)q(y - x) = E(t)q\xi = E(t)q(\xi_- + \xi_+). \quad (2.71)$$

Writing the coordinate of the first physical oscillator, in terms of reduced normal coordinates, we get

$$x = \frac{\xi_+}{\lambda_+ - 1} + \frac{\xi_-}{\lambda_- - 1}. \quad (2.72)$$

We can express, in analogy to the formula (2.1), the complete Hamiltonian of the transducing scheme when a classical force $F(t)$ is applied to the first physical oscillator:

$$\begin{aligned}
H_S = & \frac{p_+^2}{2m_+} + \frac{1}{2}m_+\omega_+^2\xi_+^2 + \frac{p_-^2}{2m_-} + \frac{1}{2}m_-\omega_-^2\xi_-^2 \\
& + H_i + \frac{\phi^2}{2L} + \frac{1}{2}L\omega_e^2q^2 \\
& - F(t) \left[\frac{\xi_+}{\lambda_+ - 1} + \frac{\xi_-}{\lambda_- - 1} \right] - qR(t). \quad (2.73)
\end{aligned}$$

It follows that the double harmonic oscillator system is described by six Hamilton equations of motion:

$$\begin{aligned}
\dot{p}_- = & -m_-\omega_-^2\xi_- - E(t)q + \frac{F(t)}{\lambda_- - 1}, \\
\dot{\xi}_- = & p_{\xi_-} / m_-, \\
\dot{p}_+ = & -m_+\omega_+^2\xi_+ - E(t)q + \frac{F(t)}{\lambda_+ - 1}, \\
\dot{\xi}_+ = & p_{\xi_+} / m_+, \\
\dot{\phi} = & -L\omega_e^2q + R(t) - E(t)(\xi_- + \xi_+), \\
\dot{q} = & \phi / L. \quad (2.74)
\end{aligned}$$

The system (2.74) is composed of two normal oscillators, of masses m_- and m_+ , and frequencies ν_- and ν_+ , both coupled in parallel to the same electrical oscillator at ν_e .

We now introduce the two components of the complex amplitudes Ξ_- and Ξ_+ of the reduced normal coordinates ξ_+ and ξ_- :

$$\begin{aligned}
\Xi_{-2} + j\Xi_{-1} = & (1/\omega_-)(\dot{\xi}_- + j\omega_-\xi_-)e^{-j\omega_-t}, \\
\Xi_{+2} + j\Xi_{+1} = & (1/\omega_+)(\dot{\xi}_+ + j\omega_+\xi_+)e^{-j\omega_+t}, \quad (2.75) \\
Q_2 + jQ_1 = & (1/\omega_e)(\dot{q} + j\omega_e q)e^{-j\omega_e t}.
\end{aligned}$$

Substituting these expressions in Eq. (2.79), we get the analogue of the system (2.5):

$$\begin{aligned}
\dot{\Xi}_{-1} = & \frac{E(t)}{m_-\omega_-} \sin\omega_-t \cos\omega_e t Q_1 + \frac{E(t)}{m_-\omega_-} \\
& \times \sin\omega_-t \sin\omega_e t Q_2 - \frac{F(t)}{m_-\omega_-} \frac{\sin\omega_-t}{\lambda_- - 1}, \\
\dot{\Xi}_{-2} = & -\frac{E(t)}{m_-\omega_-} \cos\omega_-t \cos\omega_e t Q_1 - \frac{E(t)}{m_-\omega_-} \\
& \times \cos\omega_-t \sin\omega_e t Q_2 + \frac{F(t)}{m_-\omega_-} \frac{\cos\omega_-t}{\lambda_- - 1}, \\
\dot{\Xi}_{+1} = & \frac{E(t)}{m_+\omega_+} \sin\omega_+t \cos\omega_e t Q_1 + \frac{E(t)}{m_+\omega_+} \\
& \times \sin\omega_+t \sin\omega_e t Q_2 - \frac{F(t)}{m_+\omega_+} \frac{\sin\omega_+t}{\lambda_+ - 1}, \\
\dot{\Xi}_{+2} = & -\frac{E(t)}{m_+\omega_+} \cos\omega_+t \cos\omega_e t Q_1 - \frac{E(t)}{m_+\omega_+} \\
& \times \cos\omega_+t \sin\omega_e t Q_2 + \frac{F(t)}{m_+\omega_+} \frac{\cos\omega_+t}{\lambda_+ - 1},
\end{aligned}$$

$$\begin{aligned}
\dot{Q}_1 = & \frac{E(t)}{L\omega_e} \cos\omega_-t \sin\omega_e t \Xi_{-1} + \frac{E(t)}{L\omega_e} \sin\omega_-t \sin\omega_e t \Xi_{-2} \\
& + \frac{E(t)}{L\omega_e} \cos\omega_+t \sin\omega_e t \Xi_{+1} \\
& + \frac{E(t)}{L\omega_e} \sin\omega_+t \sin\omega_e t \Xi_{+2} \\
& - \frac{R(t)}{L\omega_e} \sin\omega_e t, \\
\dot{Q}_2 = & -\frac{E(t)}{L\omega_e} \cos\omega_-t \cos\omega_e t \Xi_{-1} \\
& - \frac{E(t)}{L\omega_e} \sin\omega_-t \cos\omega_e t \Xi_{-2} \\
& - \frac{E(t)}{L\omega_e} \cos\omega_+t \cos\omega_e t \Xi_{+1} \\
& - \frac{E(t)}{L\omega_e} \sin\omega_+t \cos\omega_e t \Xi_{+2} + \frac{R(t)}{L\omega_e} \sin\omega_e t. \quad (2.76)
\end{aligned}$$

In this new configuration we choose a pump field with a spectral composition suitable for BAE pumping of both normal modes:

$$E(t) = E_0 \cos\omega_e t \cos\omega_+ t + E_0 \cos\omega_e t \cos\omega_- t \quad (2.77)$$

and the interaction Hamiltonian H_i in terms of the complex amplitudes (averaging over periods greater than $2\pi/\omega_+$, $2\pi/\omega_-$, $2\pi/\omega_e$) is

$$\begin{aligned}
\bar{H}_i \simeq & E_0 Q_1 [\Xi_{+1}(\lambda_+ - 1) + \Xi_{-1}(\lambda_- - 1)] \\
= & E_0 Q_1 (Y_1 - X_1). \quad (2.78)
\end{aligned}$$

This must be compared with the equation (2.6) derived in the case of the single mechanical oscillator. In a similar way it can be easily shown from Eqs. (2.76) that a perturbation on Q_2 acts on both Ξ_{+1} and Ξ_{-1} . A scheme of the relations between the six variables is shown in Fig. 4.

III. THE DIFFERENTIAL RESONANT CAPACITIVE TRANSDUCER

A. Basic requirements

for a parametric resonant capacitive transducer

The push-pull motion transducer is the main element of a BAE scheme. The constraints on the design of the transducer can be derived from the T_{eff} equation (2.54) which gives the sensitivity of our apparatus to energy

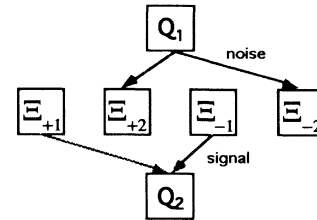


FIG. 4. Relations between BAE variables in a double oscillator-detection scheme.

variations. We summarize here the following constraints: (a) balancing as good as possible of its two capacitances; (b) high mechanical merit factor Q_m ; (c) high electrical merit factor Q_e ; (d) high polarizing electrical field E_0 . Moreover, we plan to use the transducer at low temperature in order to reduce the noise due to the Brownian motion of the mechanical mode of the system. Indeed, the use of low temperatures is advantageous concerning the mechanical and electrical quality factors. The mechanical Q of the aluminum alloy Al 5056, used for the cryogenic GW detectors, increases by a factor of 100 from room temperature to 10 K [21]. Below 1 K this alloy is superconductive and we expect that the electrical losses in the transducer are reduced [22]. On the other hand, the electrical losses of the insulating material that we use in our capacitor (Teflon PTFE) are reduced by a factor of at least 100 from room temperature to 4 K [23]. However, the construction of a low-temperature device implies severe technical constraint on its design, in particular to obtain a good balance between the two active capacitances of the transducer.

In the next section we describe our resonant transducer designed to operate at low temperatures.

The system (2.76) also shows that at the output of our circuit we can measure one phase of our electrical variable (e.g., Q_1) which brings the information carried by both the phases $\hat{\Xi}_{+2}$ and $\hat{\Xi}_{-2}$ of complex amplitudes of the normal modes. The behavior of each normal mode with respect to noise will be the same as for a single oscillator system. However, because of the intrinsically nonlinear nature of the transduction circuit, a more strict constraint will arise regarding the overall value of Q_e . In fact, at the system output we also have two Fourier components at the frequencies $\omega_e - (\omega_+ - \omega_-)$ and $\omega_e + (\omega_+ - \omega_-)$. This implies that, in order to reduce the analysis of the noise of the system to the same case of the single mechanical oscillator, the electrical circuit must be so selective that we can assume that its contribution is negligible. In other words we must have

$$Q_e \gg \frac{\omega_e}{2(\omega_+ - \omega_-)}. \quad (2.79)$$

It also follows that the noise performances of the resonant transducer can be derived by treating each vibration as independent, and defining a signal-to-noise ratio for each mode. In this way the complete analysis presented in Sec. II E, regarding the single harmonic oscillator system, is extended to the resonant transducer configuration.

The exact calculation of the signal-to-noise ratio (SNR) at the output of a double oscillator system requires a more complex and extensive analysis that will be presented elsewhere.

B. Development of the transducer

To develop the push-pull transducer we have taken advantage of the experience gained in the construction of the resonant capacitive transducer of the Rome group GW antenna (GWA) [13]. This approach was suggested by the good performance of this transducer at low temperatures with reference to the high mechanical quality factor, the easy tuning of its flexural frequency with the

resonant frequency of the antenna and its low electrical losses [24].

The resonator is a disk fixed at the inner radius and free at the outer radius vibrating in its first flexural mode. The vibrating plate has the shape of a mushroom whose shank has a larger diameter in the terminal part which is threaded in order to fasten it on a heavy mass. Particular care was taken in the design of the clamping part to ensure a rigid mechanical coupling and to keep the surfaces of the disk parallel to the base within the tolerances.

This vibrating body is the central plate of the push-pull capacitor. The other electrodes are two rings of equal sizes, within the mechanical tolerances, one rigidly fastened with eight bolts on the base and the other one on the lid of the transducer. These electrodes are insulated by means of Teflon PTFE washers. In order to minimize the stray capacitances the two rings are shaped in such a way as to have a minimum contact area and a larger vacuum gap between them and the outer shell (base and lid) of the transducer.

The main body of the transducer is made of Al alloy 5056 which shows a steep increase of the Q value at low temperatures and has a superconducting transition temperature of 0.9 K [22]. The lid and the base are locked together by four brass bolts having a thermal contraction coefficient near that of Al. The remaining difference in thermal contractions between transducer and bolts is compensated by means of four stainless-steel tubes of suitable dimensions. Before the assembly, all the components of the transducer were cooled down at liquid nitrogen temperature several times to prevent plastic deformations during the subsequent thermal cycles. When the electrode rings are locked on the base and on the lid of the transducer, electrically insulated by means of the PTFE washers, the two stray capacitances between the electrodes and their supports are measured. After a check of the surface parallelism, the vibrating disk is rigidly clamped on the base. Then the capacitance between the disk, assembled on the base, and the electrode is measured and the value of the achieved gap deduced. In order to obtain an equal gap between the vibrating disk and the second electrode ring we remove a suitable thickness from the lid and we measure the value of the two capacitances after every machining. This procedure is repeated several times until a relative difference of the two capacitances lower than the accuracy of the available impedance bridge (10^{-4}) is obtained. The assembly is made in a class 100 clean room to avoid the accidental insertion of dust particles in the two gaps. This procedure was followed to build a transducer suitable for the 2270 kg cryogenic gravitational wave antennas of the Rome group [24,25] (Fig. 5).

The resonator is a disk of 17.0 cm diameter and 0.65 cm thickness, having a mass of 380 g. The whole body of the transducer has a weight of 11 kg. Before a thermal cycle at liquid helium temperature the two capacitances of the assembled transducer had both the value $C = (1780 \pm 1)$ pF with a value of the stray capacitances of $C_s = (132 \pm 1)$ pF equal for both the electrodes.

From these data we deduce a relative difference of the two stray capacitances less than 10^{-3} and a value of the

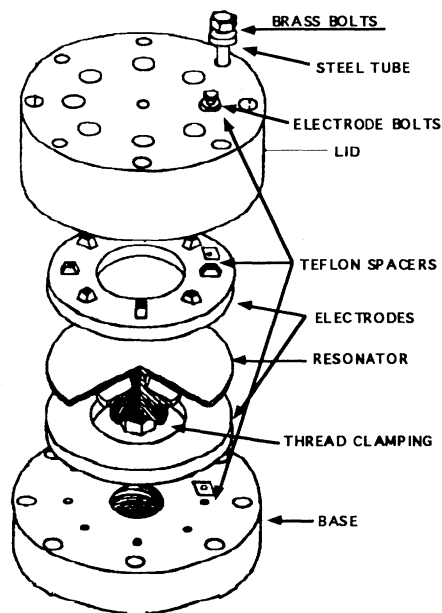


FIG. 5. Exploded view of the differential capacitive resonant transducer.

two gaps of $D = (92.4 \pm 0.1) \mu\text{m}$ which gives an upper limit for their relative difference $\rho_d < 10^{-3}$. The machining tolerances of the surfaces insure an upper limit for their relative difference $< 10^{-4}$.

C. Test of the transducer at low temperatures

We tested the behavior of the transducer at low temperatures measuring its main electromechanical characteristics before its insertion in the detection circuit. The tests were performed suspending the transducer in a vertical cryostat by means of a compact double stage low dissipation support described in Ref. [26].

We measured the frequency and the quality factor of the first flexural symmetric mode of the transducer and the values of the two capacitances at room, liquid nitrogen, and liquid helium temperature. The results are summarized in Tables I and II.

Table I shows that a lower limit for the mechanical $Q \approx 2.8 \times 10^6$ has been obtained at liquid helium temperature. Though a great amount of effort has been spent in avoiding any additional mechanical loss, we cannot exclude any influence on the measured value of Q by the dissipation of the support and cryogenic housing of the transducer. In any event, comparing the result with the

TABLE I. Measured values of Q and frequency of the push-pull resonant transducer as a function of temperature.

$T(K)$	ν_i (Hz)	Q_i
293	880.75 ± 0.06	$(7.5 \pm 0.2) \times 10^3$
77	924.38 ± 0.06	$(1.1 \pm 0.1) \times 10^5$
4.2	927.86 ± 0.06	$(2.80 \pm 0.05) \times 10^6$

TABLE II. Variation of the capacitances of the push-pull transducer as a function of temperature.

T (K)	$10^{-2} \frac{\Delta C_1}{C_1}$	$10^{-2} \frac{\Delta C_2}{C_2}$	$10^{-2} \frac{2(C_1 - C_2)}{C_1 + C_2}$
293			3.5 ± 0.2
77	$-(3.1 \pm 0.1)$	$-(0.4 \pm 0.1)$	6.3 ± 0.2
4.2	$-(3.1 \pm 0.01)$	$-(0.8 \pm 0.1)$	5.9 ± 0.2
293	$-(1.1 \pm 0.01)$	$-(0.6 \pm 0.1)$	4.0 ± 0.2

value $Q \approx 3 \times 10^6$ measured on the single electrode transducer [24], we consider it satisfactory.

Table II shows that the capacitances measured with the impedance bridge change by 1% for one and 3% for the other while cooling from 300 to 4.2 K. We point out that these values of $\Delta C/C$ also include the variations of the stray capacitances given by the insulating Teflon washers and by the signal pickup cables.

An alternative method of unbalance measurement which should not be affected by stray capacitance variations was carried out at 77 K. The resonator is excited at its resonance frequency to a known amplitude x and the two capacitances of the transducer are biased in parallel at a constant charge with an electric field E . It can be easily shown that, if the approximation $\bar{x}^2/d^2 \ll \Delta C/C$ is valid and $\rho_a \ll \rho_d$, this configuration gives an ac output voltage:

$$V_{\text{out}_a} = E(\Delta C/C)x. \quad (3.1)$$

On the other hand, if only one of the two capacitances of the transducer is biased with E the ac output voltage is given by $V_{\text{out}_b} = Ex$. Thus the value of $\Delta C/C$ is obtained from the relation

$$\Delta C/C = V_{\text{out}_a} / V_{\text{out}_b}. \quad (3.2)$$

We repeated this kind of measurement for different values of vibration amplitudes and found consistently $\Delta C/C = (4.2 \pm 0.2) \times 10^{-3}$. It follows that a consistent fraction of the residual output is due to the difference in the parasitic capacitances.

IV. THE BRIDGE READOUT CIRCUIT

A. Development of the passive elements

In the preceding section, we have seen that the two capacitances of the transducer have a difference of the order of 1% at low temperature. This is also the order of the balance which can be reached by the machining precision of the different parts of the transducer. However, this value is largely insufficient to decrease the noise of the polarizing pumps to a level suitable to have a good sensitivity; so it is necessary to be able to adjust the balance at low temperature, by means of a variable capacitor inserted in one arm of the bridge. However, it must be considered that such a device must satisfy four stringent conditions.

(a) It must operate properly at liquid helium temperature.

(b) The device must be remote controlled. In fact, the transducer is meant to be used on a cryogenic GW antenna, where no direct access to the experimental space is possible from outside.

(c) It must have a high value of Q_e , in order not to degrade the performance of the system and satisfy condition (2.79).

(d) The variable capacitance must be able to compensate at least the unpredictable variation of the capacitances of the transducer (≈ 50 pF) and have a resolution sufficient to reach a balance of at least 10^{-6} .

This last condition is the most difficult to satisfy with just one device. In practice, two variable capacitances have been developed. The first one has a resolution of ≈ 1 pF and a range of $\approx \pm 100$ pF, and the second one has a range of $\approx +5$ pF and a resolution 10^{-3} pF.

1. The wide range variable capacitor

The wide range variable capacitor is composed of two coaxial cylinders butterfly shaped and made of stainless-steel AISI 304L. The inner one can be rotated by a dc electrical motor through a high gain gear. We used the gear to have a very slow variation of the capacitance and to improve the resolution of the capacitance.

No dielectric has been used into the gap in order to keep the electrical losses at the minimum. Where necessary, Teflon PTFE has been used to insulate the two armatures from the support and from the driving gear.

In view of low-temperature operation, the construction and the assembling procedures of the capacitance are rather complex. Both the electrical motor and the driving gear have been carefully modified to operate at 4 K with good reliability: The variable capacitance can be schematized as a parallel of three terms: a fixed stray capacitance, plus two variable capacitors, one with parallel plane plates, and one with cylindrical armatures:

$$C_{\text{var}} = C_p + \frac{1}{2} \left[\frac{2\pi\epsilon_0 L}{\ln(r_1/r_2)} + \frac{\epsilon_0\pi r_2^2}{d} \right], \quad (4.1)$$

where d is the gap of the plane capacitance, L is the length of the cylindrical capacitances, and r_1 are the outer and inner radius of the cylindrical armatures.

In our prototype we have $L = 36$ mm, $r_1 = 31$ mm, $r_2 = 30.8$ mm, and $d = 100$ μm , so that the gap of the cylindrical capacitance is 200 μm ; the gap of the plane capacitance is 100 μm . These values require a high machining precision, because the entire structure is supported only along the axis. Moreover, the dimensions of the capacitance support and those of the case of the driving assembly had to be carefully gauged in order to take into account the different thermal contractions of the motor and the gear.

Once assembled, the capacitance has been tested at liquid nitrogen temperature before its insertion in the bridge circuit and we measured a capacitance change of 18 pF from room temperature to 77 K. At 77 K the interval of variation of the capacitance is 56 pF $< C_{\text{var}} < 308$ pF. We drive the motor with a voltage as low as 0.4 V obtaining a variation velocity:

$$\Delta C / \Delta t = 0.1 \text{ pF/s}.$$

This rate permits us to achieve a balance factor $\eta_z = \Delta C / C \approx 10^{-4}$. In order to achieve a better value of η_z a high-resolution variable capacitance has been developed.

2. The high-resolution variable capacitance

The high-resolution variable capacitance is a parallel plate capacitor having one armature driven by a piezoelectric ceramic stack. A piezoelectric ceramic gives a very sensitive way to vary the gap of the capacitance; however, its efficiency decreases from room to liquid helium temperature. This imposes a constraint on the maximum value of the gap allowed in order to have a variation range of the order of 1 pF. On the other hand, piezoelectric ceramics have thermal contraction coefficients an order of magnitude smaller than those of the metals as the stainless-steel AISI 304. As a consequence a high machining precision is also required in this case, in particular for the external container of the piezoelectric and the capacitance armature support. In this way the various components are assembled accurately taking care of the different thermal contractions of the various materials, so that the capacitor gap, wide at room temperature, is reduced at a predetermined value at 4 K. Moreover, the piezoelectric stack is provided with a return spring, gauged in such a way as to ensure the appropriate compression at low temperature and to avoid mechanical creeps in the ceramic.

In this device as in the case of the wide range variable capacitor, Teflon PTFE was used to insulate all the parts of the piezoelectric variable capacitor. The mobile armature of the variable capacitor is connected to the end of the piezoelectric stack by means of a fiber glass support that is easier to machine than the Teflon PTFE and permits us to define a more accurate position of the armature. The variable capacitance is a function of the bias voltage of the piezoelectric stack:

$$C(V_{\text{pz}}) = C_p + \frac{\epsilon_0 S}{d_0 - \alpha V_{\text{pz}}}, \quad (4.2)$$

where S is the surface of the capacitor, d_0 is the gap, and α is the transduction factor (in m/V) of the piezoelectric polarized with tension V_{pz} .

In Fig. 6 the variation of capacitance at room, liquid nitrogen, and helium temperature as a function of V_{pz} is shown. The data taken at 293 and 77 K reported in the figure were obtained by a direct measurement of the capacitance of the device. At 4.5 K the device was inserted in the bridge circuit and the data shown are derived from the variation of the resonance frequency of the electrical circuit as a function of V_{pz} .

It can be seen that the efficiency of the variable capacitance increases from room to liquid nitrogen temperature. This is due to a corresponding decreasing value of the gap of the active capacitance, while the value of α in the two cases is comparable. The gap is ≈ 700 μm at room temperature and becomes ≈ 250 μm at 77 K.

As the temperature decreases down to 4.5 K, the effect

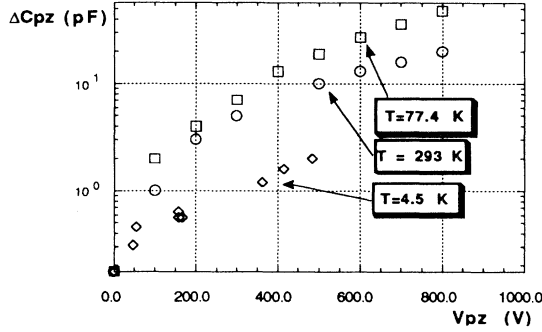


FIG. 6. Plot of the variation of the high-resolution variable capacitance as a function of temperature.

of the thermal contraction is not relevant any more but the efficiency of the piezoelectric stack decreases. As a consequence, the value of α decreases by an order of magnitude and the efficiency of the variable capacitance varies accordingly. However, it can be seen that the capacity has a variation of 2 pF with $V_{pz}=484$ V at 4.5 K. This value is largely sufficient to finely balance the bridge, complementing the coarser action of the wide range variable capacitor.

3. The other elements of the bridge

The complete scheme of our transducing configuration is shown in Fig. 7, including some auxiliary components that are described below. The readout electrical circuit is also equipped with other capacitors to complete the bridge and to match, wherever necessary, the values of the variable capacitors, approaching the bridge balance. These capacitors have been constructed following the same criteria of the variable ones. Stainless-steel plates are closed on a vacuum gap, using small washers of Teflon PTFE as spacers. Dimensions of all these elements are chosen to have mechanical resonances far from the vibration frequency of the transducer.

In order to ensure an electrical Q as high as possible, the readout coil at the central arm of the bridge is made of a pure niobium wire 0.5 mm in diameter insulated with a layer of Teflon PTFE 125 μm thick. The coil is wound

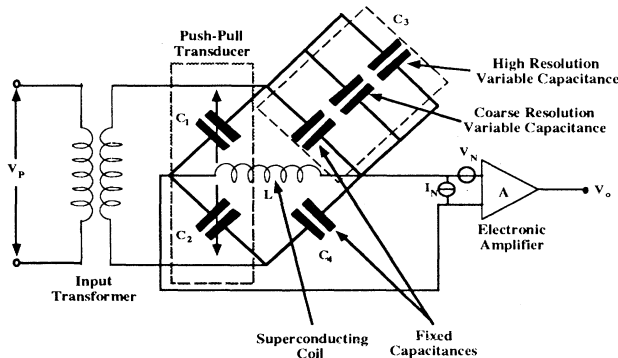


FIG. 7. Scheme of the complete transducing configuration.

around a Teflon core, and is set inside a double layer lead superconducting shield. Being the capacity of the transducer ≈ 1.5 nF, we have wound a 1 mH superconducting coil to get the electric frequency in the region of 100 kHz. This frequency was chosen for ease of operation and instrumentation, although an eventual move to higher values will be made to improve sensitivity.

The em pumps are connected to the electrical circuit through a transformer that increases the input voltage. The superconducting transformer with ratio 1:5.5 is made in the same way as the central arm coil.

All these various elements of the circuit are electrically connected using NbTi superconducting wires and Nb superconducting contacts. In parallel to the superconducting wires we set a normal copper wire, having the same overall length for each arm of the bridge in order to be able to check the bridge balance before cooling to 4.2 K.

V. MEASUREMENTS ON THE SYSTEM AT LOW TEMPERATURE

A. Measurement of the characteristics of the apparatus and of the static balance

The complete system has been assembled and several runs have been performed at liquid helium temperature, using our transducer test facility [26]. The main purpose of the test runs is the noise measurement of the transducing system in order to verify the theoretical model, and confirm the feasibility of the back-action-evasion technique. The balancing of the bridge is crucial to this purpose.

The first step in the procedure of bridge balance is to measure the mechanical frequencies and merit factor of the transducer and the electric frequency and quality factor of the readout circuit. Then a monochromatic signal is sent to the bridge at ν_e , and the corresponding output is measured. The resulting balance is given by the knowledge of the transfer function of the circuit, as expressed for instance by (4.2). In the case of monochromatic excitation the η_z expression is well approximated as

$$\eta_z = \frac{V_{\text{out}}}{V_{\text{in}} G N_t Q_e}, \quad (5.1)$$

where N_t is the turn ratio of the input transformer, G the gain of the electronic amplifier at the output of the readout circuit, and V_{in} is the amplitude of the monochromatic signal at the input. We checked the accuracy of the η_z measure done throughout the electrical bandwidth and we verify that spurious couplings between input and output are absent in the system.

As an example we report in Fig. 8 the electrical resonance curve $\nu_e = 123$ kHz that corresponds to a value of $\eta_z \approx 10^{-5}$ with an electric quality factor $Q_e = 6300$.

We notice that this Q_e value is sufficient to fulfill the condition (2.74) in the case of the cryogenic antennas Nautilus and Explorer. In fact, in both cases the distance between the two normal modes is $\nu_+ - \nu_- \approx 17$ Hz [25,27], which gives the inequality $Q_e > 3500$. The balance is optimized using the variable capacitors, as dis-

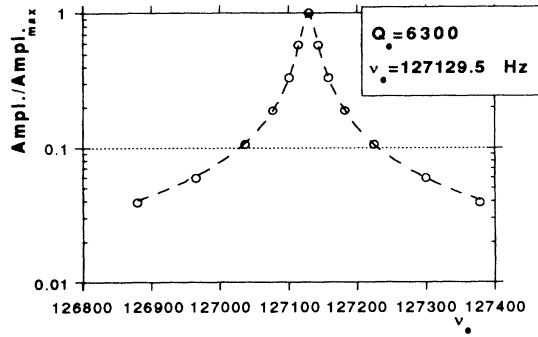


FIG. 8. Transfer function of the electrical resonance of the circuit.

cussed in the previous sections: the optimum point is approached with the motor driven variable capacitor, and then the piezoelectric stack capacitor is activated and the minimum value of η_z achieved.

In Fig. 9 we show the best result we have obtained, with a value of $\eta_z = 8 \times 10^{-7}$. We stress that this result has come out to be reproducible, and has been obtained repeatedly in our last measurement run. Reliability is crucial in view of the use of the apparatus on a real cryogenic gw antenna, that has a cycling time of several months.

B. The noise output of the transducer

Once the optimum balance point has been reached, the apparatus can be biased in the BAE scheme and a measurement of the output noise can be attempted. We have biased the transducer using a commercial double synthesizer Hewlett Packard HP 3326A, with a maximum amplitude at the input of the bridge of $5V_{pp}$. The signal at the output is amplified by a commercial PAR 113 amplifier and the two phases extracted by a lock-in. The reference of the lock-in uses the same master oscillator of the two pumps, to maintain the same relative phase reference during data acquisition. The data are sampled and stored using a Macintosh II computer equipped with a Metrabyte analogue-to-digital converter (ADC) board.

In Fig. 10 we show a typical spectrum at the output, in

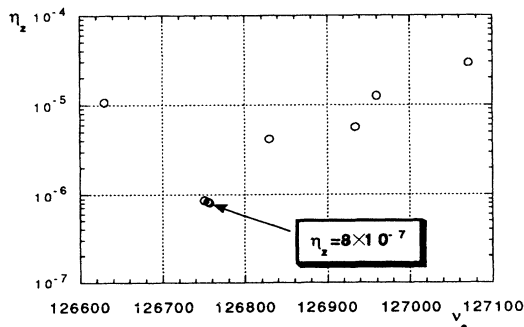


FIG. 9. Balance of the bridge vs frequency. Each value of v_e corresponds to a different setting of the two variable capacitances.

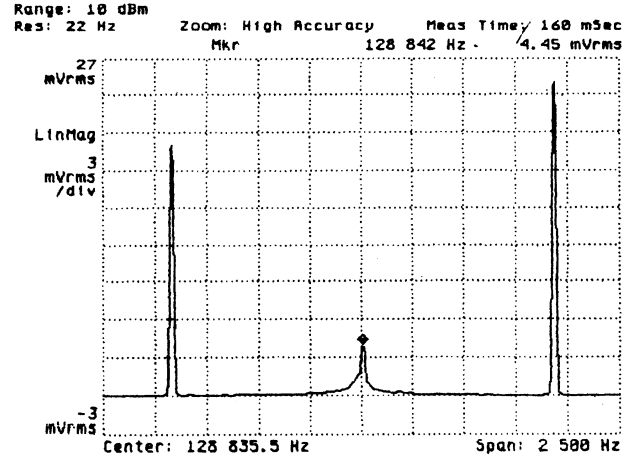


FIG. 10. Spectrum of the output of the transducer. Two noise components can be recognized: the white noise due to the amplifier and the wide band noise at the electrical resonance. Because of the imperfect balance, at Ω_- and Ω_+ are the residual peaks due to the biasing pumps.

which the white band noise of the amplifier and the wide band noise at the electrical resonance are due to the pumps. Because of the imperfect balance, the two peaks due to the biasing pumps at $\Omega_- = \omega_e - \omega_m$ and $\Omega_+ = \omega_e + \omega_m$ are present. During our measurement runs we have recorded about 50 h of data, in different experimental conditions.

We show in Fig. 11 the plot of the two phases of the transducer output when the mechanical oscillator is excited well above the noise level. As is shown by Eq. (2.26), the transducer signal is only in one phase of the output.

In Fig. 12 the same data are used to fill a tridimensional histogram. Note that the scale on the V_1 axis is small-

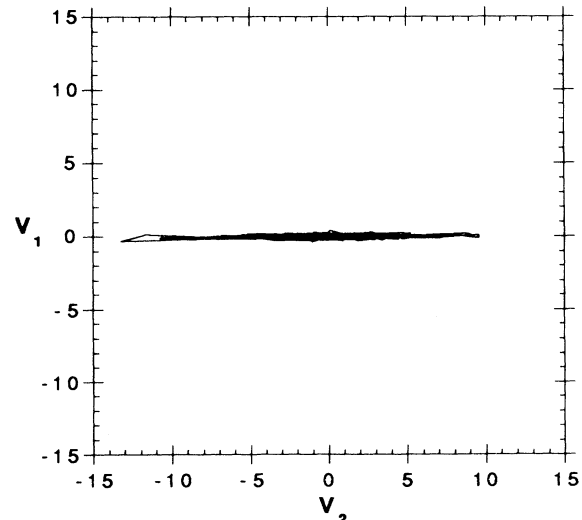


FIG. 11. Plot of the output of the transducer, with the mechanical oscillator excited well above the noise level.

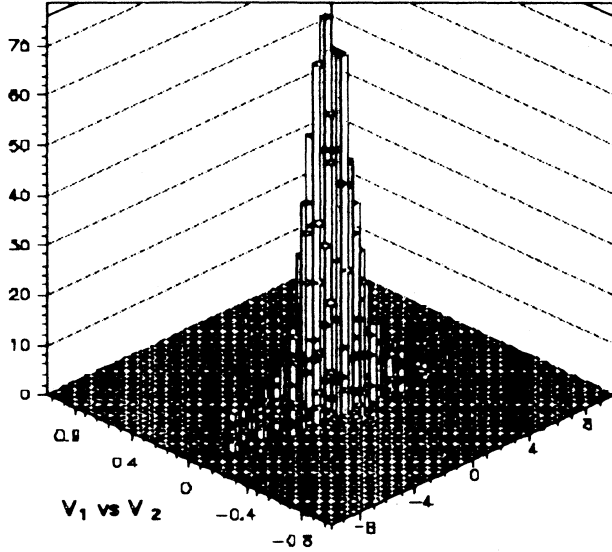


FIG. 12. The same data of Fig. 11 viewed as a 3D histogram.

er by a factor 10 than the scale on the V_2 axis. As expected, the plot shows a Gaussian behavior of the noise along the V_1 and V_2 axis with greatly different values for the standard deviation. The corresponding figure for a linear transducer would have been a Gaussian-shaped bell with a circular section along the Z axis.

In this run the transducer was excited by spurious acoustic sources at amplitudes about 100 times above the Brownian level because of an insufficient acoustic isolation. However, the signal on the *electrical* phase V_1 , which is insensitive to the mechanical excitation, behaves according to the theoretical predictions of our model, with $\eta_z = 2 \times 10^{-6}$. In Fig. 13 the experimental distribution of the V_1^2 variable is presented, where the dotted line is the distribution fit performed using the function.

The resulting value of the standard deviation is

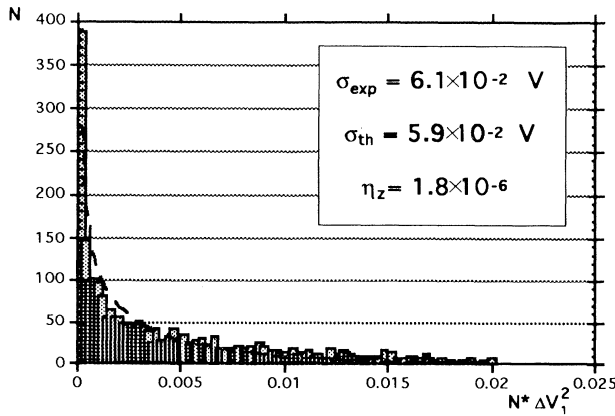


FIG. 13. Histogram of the V_1^2 variable for the data of plot 11. The value of σ_{V_1} is close to that predicted by our theoretical model.

$$(\sigma_{V_1})_{\text{expt}} = 6.1 \pm 0.4 \times 10^{-2} \text{ V ,}$$

in agreement with the value

$$(\sigma_{V_1})_{\text{th}} = 6 \pm 2 \times 10^{-2} \text{ V}$$

predicted by the equations (2.49) and (2.50). When the transducer is excited only by the Brownian stochastic force and the electrical noise sources, the output spectrum is given by Eqs. (2.46) and (2.47).

In Fig. 14 we show the lego plot of the noise output of the transducer obtained with a balance of $\eta_z = 5.6 \times 10^{-6}$ and $V_0 = 7.2 V_{pp}$. The data are taken during a second measurement run after a substantial improvement in the mechanical isolation.

In this experimental setup, the dynamics of the system is dominated by the noise of the em pumps, and we cannot notice any difference between the two phases. However, the values measured on the two phases are still in good agreement with the values predicted by our model. In Figs. 15 and 16 are the distributions of the values of V_1^2 and V_2^2 . The standard deviations derived by the distribution fits are compared with the values predicted by our model:

$$(\sigma_{V_1})_{\text{th}} = 1.5 \pm 0.4 \times 10^{-2} \text{ V ,}$$

$$(\sigma_{V_1})_{\text{expt}} = 1.2 \pm 0.2 \times 10^{-2} \text{ V ,}$$

$$(\sigma_{V_2})_{\text{th}} = 1.6 \pm 0.4 \times 10^{-2} \text{ V ,}$$

$$(\sigma_{V_2})_{\text{expt}} = 1.6 \pm 0.2 \times 10^{-2} \text{ V .}$$

In the lego plot of Fig. 17 we present the results obtained during the run in which the best transducer sensitivity was obtained. In Table III we summarize all the

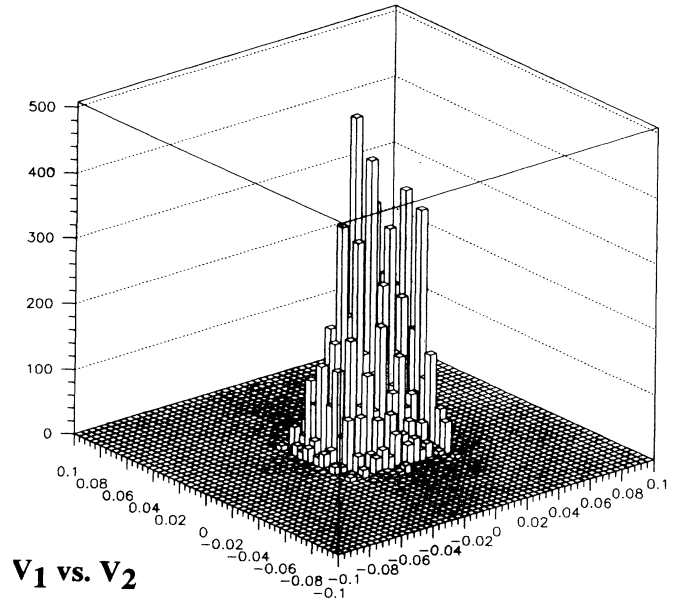


FIG. 14. 3D histogram of the output of the transducer with $\eta_z = 5.6 \times 10^{-6}$.

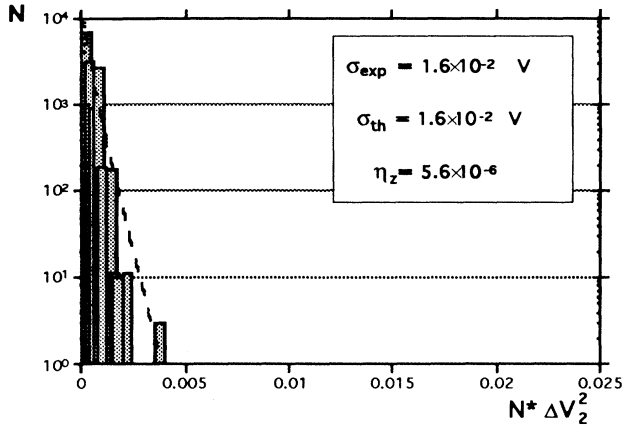
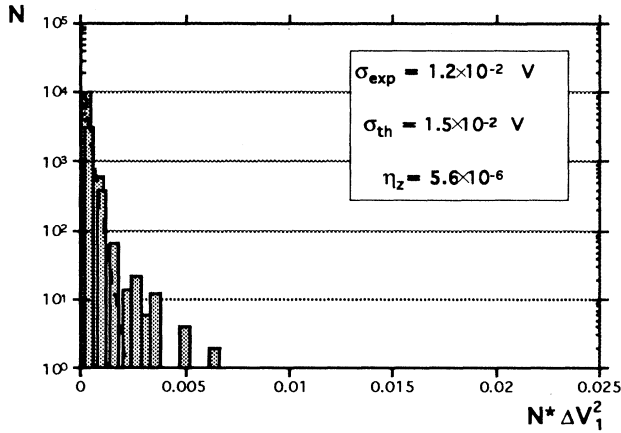
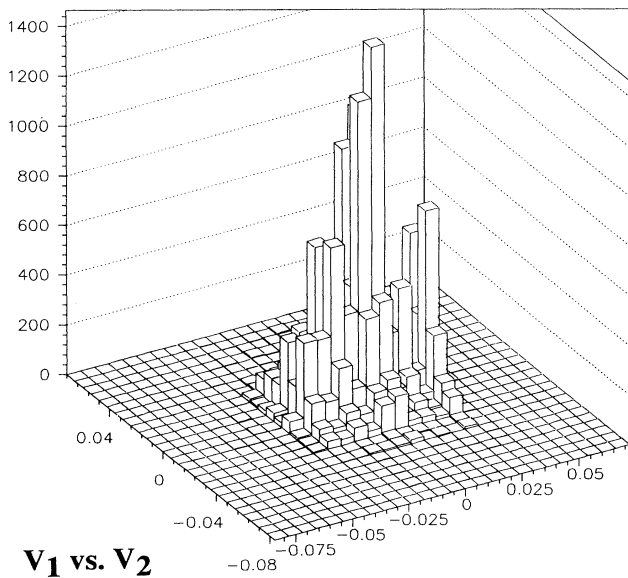
FIG. 15. Distribution of V_1^2 for the data of Fig. 14.FIG. 16. Distribution of V_2^2 for the data of Fig. 14.FIG. 17. 3D histogram of the output of the transducer with $\eta_z = 8 \times 10^{-7}$.

TABLE III. Parameters of the system during the run in which the best transducer sensitivity was obtained.

$\nu_m = 927.867$ Hz	$SV_n = 2 \times 10^{-16}$ V ² /Hz
$m_t = 0.314$ kg	$SI_n = 2 \times 10^{-28}$ A ² /Hz
$Q_m = 927000$	$S_\phi = 7.3 \times 10^{-10}$ V ² /Hz
$\nu_e = 126757.2$ Hz	$S_a = 1.1 \times 10^{-12}$ V ² /Hz
$Q_e = 6300$	
$C = 1.6$ nF	
$V_0 = 15.5$ V	
$\eta_z = 8.3 \times 10^{-7}$	
$T = 4.5$ K	

parameters of this run of measurements.

In Figs. 18 and 19 the distributions of the V_1^2 and V_2^2 are reported. As for the previous experimental results, we compare the values predicted by the model with the variances derived by the distribution fits:

$$(\sigma_{V_1})_{th} = 5 \pm 1 \times 10^{-3} \text{ V},$$

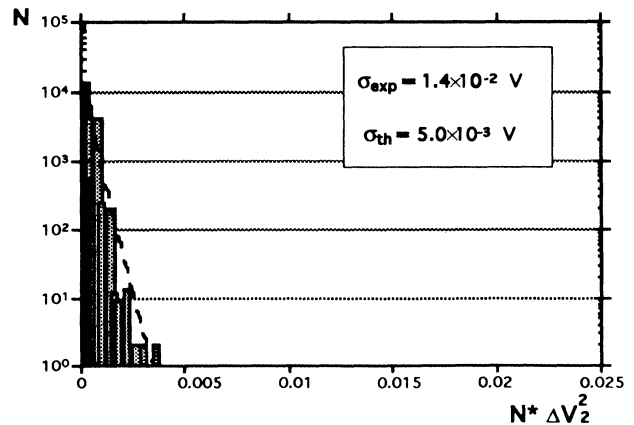
$$(\sigma_{V_1})_{expt} = 8.5 \pm 0.2 \times 10^{-3} \text{ V},$$

$$(\sigma_{V_2})_{th} = 5 \pm 1 \times 10^{-3} \text{ V},$$

$$(\sigma_{V_2})_{expt} = 14 \pm 2 \times 10^{-3} \text{ V}.$$

Also in this case we expect that the dominant noise is still due to the HP 3326A synthesizers (em pumps). We notice that the agreement between the experimental and the theoretical variance of the *electrical* phase is satisfactory, while the phase which also carries information on the mechanical motion of the transducer is higher than the expected value by a factor 3. This can again be easily explained with spurious mechanical noise exciting the transducer above its Brownian level, because the mechanical isolation of the transducer, although improved, is again not sufficient for the higher sensitivity configuration. However, we notice that the noise measured on the electrical phase is, as expected, much inferior to the value typical of a linear transduction scheme.

Indeed, using the parameters of Table III, it is easy to calculate [28] the sensitivity of a linear transducer biased with a constant electrical field of the same amplitude used

FIG. 18. Distribution of V_1^2 for the data of Fig. 17.

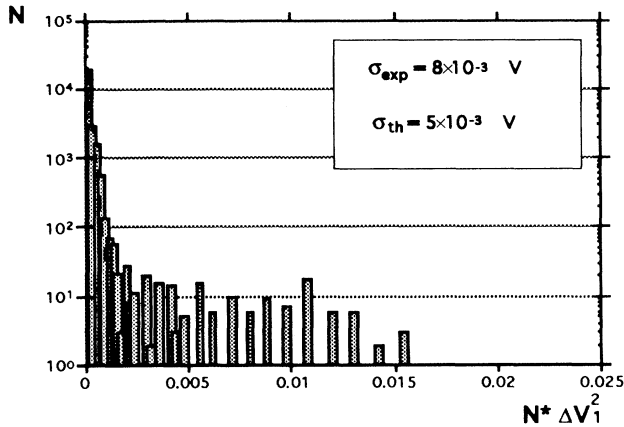


FIG. 19. Distribution of V_2^2 for the data of Fig. 17.

in the BAE configuration. The result is $T_{\text{eff}} = 53$ K to be compared with the expected value $T_{\text{eff}} = 0.5$ K of the BAE scheme. The gain in sensitivity of the parametric configuration with respect to the linear one is evident. However, the measured sensitivity of the transducer is given by the measured mechanical noise, not at the Brownian level due to a still poor mechanical isolation. In this case the sensitivity of the transducer for the detection of burst signals is $T_{\text{eff}} \approx 4$ K. This value is a factor 3 better than the sensitivity limit given by the noise of the PAR 113 amplifier in a linear configuration: $T_{\text{eff}} = 2T_n \approx 12$ K.

We stress that until now no particular effort has been made to optimize the sensitivity of this transduction apparatus. Our main aim has been to study the behavior of such a system and to verify that the theoretical model we developed was correct.

A first attempt has been made recently in order to improve the sensitivity of the apparatus using two low noise synthesizers Sciteq VDS-15 as em pumps. The experimental configuration was the same of the preceding runs, the biasing voltage applied to the bride was $8.8V_{pp}$, and the balance was 9.5×10^{-7} . In Fig. 20 is a spectrum of the output of the transducer biased with these new pumps. The resonance peak indicated by an arrow is due to the Brownian motion of the transducer. The amplitude of the peak gives a value of T_{eq} , as defined by (2.51), of 4.5 K, equal to thermodynamical temperature of the transducer. This demonstrates that no back action of the amplifier noise on the transducer is present. The amplitude of the peak at the electrical resonance is 20 times greater than the value predicted on the base of the S_ϕ and S_a values given by Sciteq for the two synthesizers. Further measurements will be needed to find out if this value is due to external electrical noise entering into the system and to correct this problem. No data have been taken during this first test of the new em pumps.

In the near future we plan to increase the balance of the bridge circuit by at least an order of magnitude using new variable capacitances and wiring schemes. Moreover, we are trying to reduce the noise at the source by using properly matched high Q filters. As we have noticed before, the sensitivity of the transducer is limited in

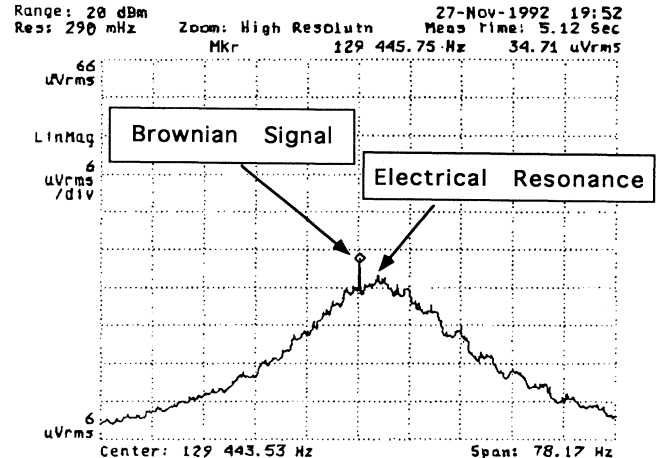


FIG. 20. Spectrum of the output of the transducer biased with new low noise pumps. The peak due to the mechanical signal of the transducer is shown. The amplitude is in agreement with the predicted value given the Brownian motion of the resonator at $T = 4.5$ K.

principle by the synthesizer noise. In the case of negligible pump noise, using a PAR 113 amplifier we could obtain $T_{\text{eff}} \approx 10$ mK. Using a noncommercial, very low noise field effect transistor (FET) amplifier [29], having $T_n \approx 100$ mK, we would achieve $T_{\text{eff}} \approx 100$ μ K. Further, we are constructing a new system, with its mechanical frequency tuned at 1.8 kHz, that is the detection frequency of the cryogenic gravitational wave antenna Altair [30] and we plan, during 1993 to perform a first test of the noise reduction techniques with a BAE system applied to a real double harmonic oscillator.

VI. CONCLUSION

We have developed and tested a low-temperature prototype of a transduction apparatus which uses a back-action-evading scheme. The prototype worked successfully, showing a high value of the mechanical Q (2.8×10^6), a satisfactory geometrical balance and a good stability of the electrical and geometrical parameters during the thermal cycles between room and liquid helium temperatures. The bridge readout circuit was balanced down to 0.8 ppm and an electrical quality factor $Q_e \approx 6 \times 10^3$ was measured at the electrical resonance frequency of 125 kHz. A first test on the noise behavior of the system shows a good quantitative agreement with a theoretical model. However, the main noise source is still due to the pumps, and limits the energy sensitivity of the transducer to $T_{\text{eff}} \approx 0.5$ K. Finally, we point out that, by improving the balance of the bridge by another order of magnitude, an energy sensitivity $T_{\text{eff}} \approx 100$ μ K could be reached. In this case, this transducer will be suitable to serve as the main element of a parametric scheme for avoiding the back action effect of the coupled amplifier.

ACKNOWLEDGMENTS

We thank D. Di Diadoro, G. Martinelli, A. Mattei, and E. Serrani for the skillful technical support.

- [1] E. Amaldi and G. Pizzella, *Relativity, Quanta and Cosmology in the Development of the Scientific Thought of Albert Einstein* (Academic, New York, 1979).
- [2] E. Amaldi, M. Bassan, P. Bonifazi, P. Carelli, M. G. Castellano, G. Cavallari, E. Coccia, C. Cosmelli, V. Foglietti, S. Frasca, I. Modena, G. V. Pallottino, G. Pizzella, P. Rapagnani, and F. Ricci, in *Proceedings of the 4th Marcel Grossmann Meeting on General Relativity*, Rome, Italy, 1985, edited by R. Ruffini (North-Holland, Amsterdam, 1986).
- [3] E. Amaldi, P. Astone, M. Bassan, P. Bonifazi, M. G. Castellano, G. Cavallari, E. Coccia, C. Cosmelli, S. Frasca, E. Majorana, I. Modena, G. V. Pallottino, G. Pizzella, P. Rapagnani, F. Ricci, M. Visco, and N. Zhu, *Europhys. Lett.* **12**, 5 (1990).
- [4] P. Rapagnani, *Astron. Astrophys.* **229**, 28 (1990).
- [5] C. M. Caves, K. S. Thorne, R. W. P. Drever, V. D. Sandberg, and M. Zimmerman, *Rev. Mod. Phys.* **52**, 341 (1980).
- [6] V. B. Braginskij, *Zh. Eksp. Teor. Fiz.* **53**, 1434 (1967) [*Sov. Phys. JETP* **26**, 831 (1968)].
- [7] V. B. Braginskij, Yu. Vorontsov, and F. Ya. Khalili, *Zh. Eksp. Teor. Fiz.* **73**, 1340 (1977) [*Sov. Phys. JETP* **46**, 705 (1977)].
- [8] V. B. Braginskij and F. Ya. Khalili, *Quantum Measurements* (Cambridge University Press, Cambridge, England, 1992).
- [9] R. Giffard, *Phys. Rev. D* **14**, 2378 (1976).
- [10] K. S. Thorne, C. M. Caves, V. D. Sandberg, M. Zimmerman, and R. W. P. Drever, in *Sources of Gravitational Radiation*, edited by L. Smarr (Cambridge University Press, Cambridge, England, 1979).
- [11] M. F. Bocko, L. Narici, D. H. Douglass, and W. W. Johnson, *Phys. Lett.* **97A**, 259 (1983).
- [12] G. W. Spetz, A. G. Mann, W. O. Hamilton, and W. C. Oelfke, *Phys. Lett.* **104A**, 335 (1984).
- [13] O. D. Augier, W. W. Johnson, and W. O. Hamilton, *Rev. Sci. Instrum.* **62**, 11 (1991); **62**, 2523 (1991).
- [14] D. Blair, *Phys. Lett.* **91A**, 197 (1982).
- [15] F. Bordoni, S. De Panfilis, F. Fuligni, V. Iafolla, and S. Nozzoli, in *Proceedings of the 4th Marcel Grossmann Meeting on General Relativity* [2].
- [16] F. Fuligni and V. Iafolla, in *Proceedings of the 3rd Marcel Grossmann Meeting on Recent Developments in General Relativity*, Shanghai, China, 1982, edited by H. Ning (North-Holland, Amsterdam, 1983).
- [17] C. Cinquegrana, thesis, University of Rome "La Sapienza," 1991 (unpublished).
- [18] M. F. Bocko, Ph.D. thesis (unpublished).
- [19] P. Rapagnani, *Nuovo Cimento* **5c**, 385 (1982).
- [20] R. Onofrio, *Phys. Lett. A* **120**, 1 (1987).
- [21] T. Suzuki, T. Tsubono, and H. Hirakawa, *Phys. Lett.* **67A**, 2 (1978).
- [22] E. Coccia and T. O. Niinikoski, *Lett. Nuovo Cimento C* **41**, 242 (1984).
- [23] *Materials and Processes for Electronics*, edited by C. A. Harper (McGraw-Hill, New York, 1987).
- [24] E. Amaldi, P. Bonifazi, P. Carelli, M. G. Castellano, G. Cavallari, E. Coccia, C. Cosmelli, V. Foglietti, R. Habel, I. Modena, G. V. Pallottino, G. Pizzella, P. Rapagnani, and F. Ricci, in *Proceedings of the 4th Marcel Grossmann Meeting on General Relativity* [2].
- [25] P. Astone, M. Bassan, P. Bonifazi, M. G. Castellano, E. Coccia, C. Cosmelli, V. Fafone, S. Frasca, E. Majorana, I. Modena, G. V. Pallottino, G. Pizzella, P. Rapagnani, F. Ricci, and M. Visco, *Europhys. Lett.* **16**, 231 (1991).
- [26] E. Majorana, P. Rapagnani, and F. Ricci, *Meas. Sci. Technol.* **3**, 501 (1992).
- [27] P. Astone, M. Bassan, P. Bonifazi, P. Carelli, M. G. Castellano, G. Cavallari, E. Coccia, C. Cosmelli, V. Fafone, S. Frasca, E. Majorana, I. Modena, G. V. Pallottino, G. Pizzella, P. Rapagnani, F. Ricci, and M. Visco, *Phys. Rev. D* **47**, 362 (1993).
- [28] E. Amaldi, P. Bonifazi, P. Carelli, G. Cavallari, E. Coccia, C. Cosmelli, G. V. Pallottino, G. Pizzella, P. Rapagnani, and F. Ricci, *Nuovo Cimento* **9C**, 51 (1986).
- [29] G. V. Pallottino and G. Vannaroni, *IEEE Trans. Meas. IM-34*, 676 (1985).
- [30] M. Bassan, P. Bonifazi, F. Bordoni, M. G. Castellano, V. Iafolla, and M. Visco, *Astron Astrophys.* **233**, 285 (1990).